arXiv:2106.06886v1 [physics.app-ph] 13 Jun 2021

Energy harvesting coil for circularly polarized fields in magnetic resonance imaging

P. Seregin,[1,*] O. Burmistrov,[1,*] G. Solomakha,[1] E. Kretov,[1] N. Olekhno,[1] and A. Slobozhanyuk[1,†]

[1] *Department of Physics and Engineering, ITMO University, Saint Petersburg, Russia*

(Dated: March 7, 2022)

Specialized RF coils and sensors placed inside the magnetic resonance imaging (MRI) scanner considerably extend its functionality. However, since cable connected in-bore devices have several disadvantages compared to wireless ones, the latter currently undergo active development. One of the promising concepts in wireless MRI coils, energy harvesting, relies on energy carried by the RF MRI field without the need for additional transmitters as in common wireless power transfer. In this letter, we propose a compact harvesting coil design based on the combination of the loop and butterfly coils that allows energy harvesting of a circularly-polarized field. By performing numerical simulations and experiments with commonly used Siemens Espree and Avanto 1.5 Tesla MRI scanners, we have demonstrated that the proposed approach is safe, efficient, does not decrease the quality of MRI images, and allows doubling the harvested voltage in contrast with linearly polarized setup.

I. INTRODUCTION

Magnetic resonance imaging (MRI) has rendered as one of the key methods in medical diagnostics. To further extend its functionality, various in-bore devices are applied, including different flexible body receive coils and sensors. However, these devices require energy supply, and powering them with wire lines can result in imaging artifacts or patient discomfort [1]. Thus, various wireless alternatives are actively studied, including wireless power transfer (WPT) [2–8], wireless MRI coil [9] and MRI energy harvesting [10]. While the WPT requires the presence of additional transmitting coils, the harvesting relies on the conversion of electromagnetic fields that are already presented in the region of interest, such as B_1 radio-frequency (RF) field, Fig. 1, thus not requiring any modifications of the MRI scanner itself.

RF harvesting setups converting the electromagnetic energy present in the surrounding environment have been readily demonstrated considering GSM [11–15], RFID [16, 17], Wi-Fi [18, 19], and LTE [20] signals. The power level of signals in the environment for the conventional wireless communication bands has a typical power density [21–24] ranging from 2 μW/m^2 to 10 mW/m^2, which is much lower than that in MRI scanner. However, in contrast to such high-frequency applications, there are several differences when considering the application of harvesting concept in MRI: (i) MRI harvesting should work at 63 MHz for 1.5 T MRI and 128 MHz for 3 T MRI, which means near-fields region due to small MRI bore areas (usual it is approximately 70 cm in diameter); (ii) MRI scanners generate RF-fields in the form of short high-power pulses up to 10 ms long; (iii) There is a large constant magnetic field B_0 present, which requires the use of non-magnetic materials; (iv) Currents flowing in the harvesting circuit should not distort the magnetic field B_1 and B_0 which can result in the image quality decrease; (v) Since MRI is a method of medical visualization, strict safety requirements should be met, including the limitation of specific absorption rate (SAR).

The general principles of energy harvesting and its application in MRI are illustrated in Fig. 1. Inside an MRI scanner, a large constant magnetic field B_0 is created, which we assume to be lower than 3 T as a body coil is needed for the energy harvesting to function, while usually, MRI setups with $B_0 > 3$ T do not feature a body coil due to its low efficiency and strong field homogeneity in the sample [25]. A body coil used for the transmission, and a local coil for the reception of echo signals from protons [26]. In the process of MRI scanning, additional pulse gradient fields $G_x(t)$, $G_y(t)$, and $G_z(t)$ are created in order to obtain a spatial resolution [27], which have typical values of mT/m [27] and produce up to 1 MW

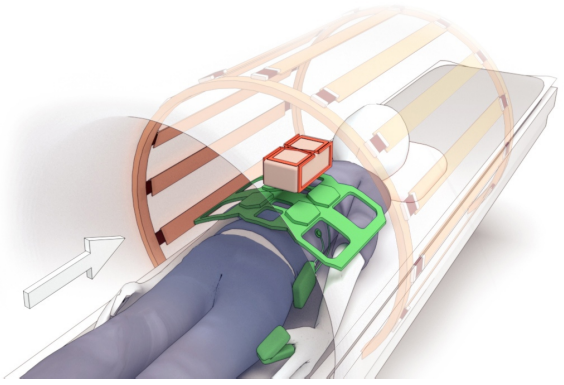


Figure 1. Artist's view of the harvesting setup. The patient located in the MRI scanner (shown with grey) with a large constant magnetic field B_0 applied. B_0 is depicted by white arrow. The harvesting coil (shown with red) is placed on top of the patient and powers up in-bore devices (shown with green) by converting the energy of RF field B_1. Examples of such equipment include local coils, heart activity monitors, and pulse sensors.

* These two authors contributed equally
† a.slobozhanyuk@metalab.ifmo.ru

of peak power [28]. However, a realization of an effective coil for their conversion is very challenging [10] since a large coil is necessary to capture spatial field variations. Finally, an RF field B_1 is created for the excitation of the nuclear magnetic resonance at the Larmor frequency [27]. This field is *circularly* polarized and has peak pulse power of 10...15 kW [29], which is potentially enough to provide DC supply for in-bore electronics, including circuits of local coils, as well as electro-cardio-graphic (ECG) gating, respiratory (chest movement tracking), and pulse (heart rate capturing) sensors of physiological signals, or external triggering source [30]. Moreover, energy harvesting coils for RF field B_1 can be effectively implemented as they do not require a large size or multi-turn design for functioning in contrast to schemes using gradient coils.

This resulted in several realizations of harvesting setups in MRI [10, 31]. However, all of the mentioned setups rely on converting linearly polarized components of the field B_1, thus limiting the harvesting efficiency. In the present letter, we extend the proposed concepts and develop a harvesting coil capable of capturing a circular polarization in order to enhance the harvesting efficiency.

II. COIL DESIGN FOR CIRCULARLY POLARIZED WAVE HARVESTING

The proposed coil concept illustrated in Fig. 2 includes two coils. One having the shape of a circle (0-shape) and another one with the shape of a butterfly (8-shape). Two coils are required to convert orthogonal linear parts of the circular polarization of the field B_1, with one linear component being captured by each coil. Considering several coil designs discussed in Supplementary Materials, we obtained the best parameters for the presented configuration. The parameters taken into account include: (i) Decoupling circuitry (additional inductors are needed for planar designs realized within a single printed circuit board, while for non-planar schemes, purely-geometrical decoupling can be applied); (ii) Conversion efficiency; (iii) Simplicity of implementation. The harvesting setup also includes two tuning capacitors, one for each coil, that are needed to precisely adjust the coil resonance to the Larmor frequency. The currents generated in coils then are rectified by voltage doublers to enhance the conversion voltage.

The value of DC current after rectifiers can reach up to relatively high values. This can lead to the emergence of an effective magnetic field disturbing the B_0 field. Since MRI requires an extreme homogeneity of B_0 field within the imaging volume, such a perturbation can result in considerable imaging artifacts [32]. To eliminate such effects, we implement all current-carrying lines in a combiner with differential pairs. Further details are given in Supplementary Materials.

The size of coil elements defines voltages obtained with harvesting setup: larger sizes result in larger voltages and harvested power, respectively. However, large sizes

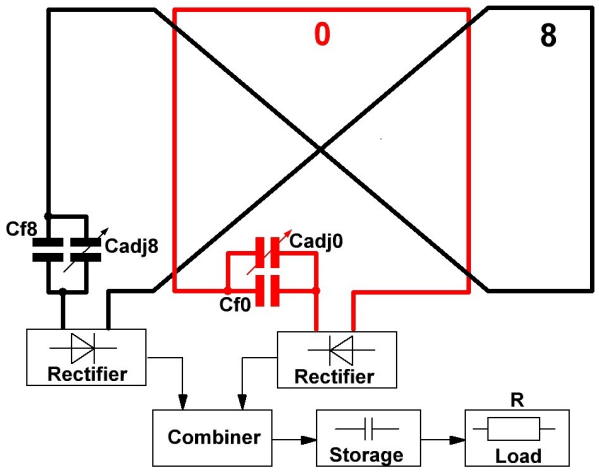


Figure 2. Schematics of the developed circularly polarized field harvesting setup consisting of two coils, one in the shape of a loop (shown in red) and another one in the shape of a butterfly (shown in black).

of harvesting coil may lead to the distortion of RF field B_1 in the vicinity of coil and decrease the patient's comfort. In experiments and numerical simulations, we use the following coil parameters: length $L = 110$ mm, width $W = 65$ mm, and height $H = 35$ mm, Fig. 3(a). Each tuning capacitor is realized as two capacitors arranged in parallel, a fixed capacitor C_f and adjustable capacitor C_{adj}. For the considered coil size, the following values are chosen: $C_f = 4$ pF and $C_{adj} = 2...12$ pF. Storage capacitor C consists of several capacitors arranged in parallel with a total capacitance of $C = 470$ μF. Two rectifiers were realized using Schottky diodes. Finally, the rectified currents from two coils are combined using RF-traps and charge the storage capacitor which powers the load 200 Ohm, which is equivalent to a load of four low noise amplifiers from a standard Siemens body flex coil.

To perform experimental studies of the developed harvesting coils with a real MRI scanners, we use the following setup illustrated in Fig. 3(b). The harvesting coil was placed at the top of a standard calibrating phantom in form of a cylindrical bottle with dimensions $520 \times 440 \times 340$ mm filled with 1,24g $NiSO_4 \times 6H_2O$/2,62g NaCl per 1000 ml distilled water. The phantom is placed upon standard pads, and together with coil located inside a cylindrical Siemens loaded body phantom MRI 5750307 filled with the same liquid. All the mentioned elements are placed on the patient table allowing to move them inside the MRI scanner.

III. EXPERIMENTAL RESULTS

We start with measuring output voltage V_{ind} induced at the load R_{load} with RF power applied to the body coil. We study the dependence of voltage V_{ind} on the distance between the harvesting coil position and the isocenter of

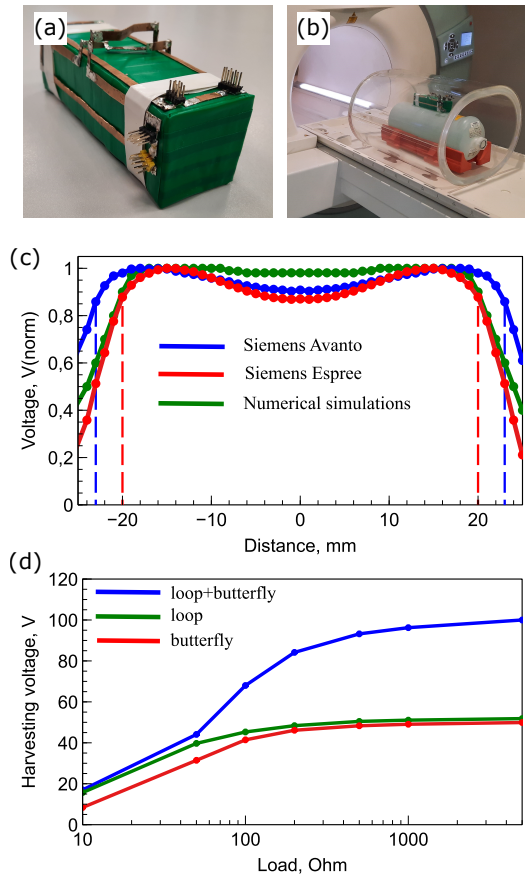


Figure 3. (a) Photo of the experimentally realized coil for circularly polarized field harvesting. (b) Experimental setup including an MRI scanner, body phantom consisting of a bottle and Siemens loading body phantom, and the harvesting coil atop of the phantom. (c) Normalized harvesting voltage value versus coil position. The region between dashed lines is suitable for harvesting. (d) Harvesting voltage value versus load resistance

MRI bore magnet z. To change the location of harvesting coil, we moved it manually while keeping the positions of the table and phantom unchanged. Such a procedure is chosen to prevent a change of the transmitting body coil impedance. The output voltage was measured using Owon XDS3202A 14-bit oscilloscope attached by a coaxial cable with multiple RF-traps to prevent cable antenna effect. We have measured the output voltage with a single excitation pulse during transmit, as RF harvesting should provide voltage to the local coil circuitry during each phase encoding step. To proceed, we applied a manual frequency adjustment procedure employing three separate pulses. However, only the first one was used to measure the output harvesting voltage. The sets of voltage measurements have been performed utilizing Siemens Avanto (red curve), Siemens Espree (blue curve) 1.5 T MRI systems and numerical simulations with CST Microwave Studio 2020 (green). The resulting voltage dependence $V(z)$ is shown in Fig. 3(c). We use geometric dimensions equivalent Espree BC for the CST numerical model.The graphs show that the width of the curves is slightly different due to the fact that the length of body coils is different. The longer the BC length, the larger the working area for harvesting can be obtained. As seen from the figure, the voltage first slowly increases when the harvesting coil is moved from the isocenter, reaching its maximum at $z \approx 14$ cm for Espree scanner and $z \approx 18$ cm for Avanto scanner. However, the voltage rapidly drops at further increase of the distance z, and the harvesting setup becomes inefficient. To estimate the region in which the harvesting setup maintains stable functionality, we select a 15% drop in the output voltage as a criterion. Then, as showed by dashed lines in Fig. 3(c), the realized harvesting coil can be freely moved within ± 20 cm range for Espree setup and within ± 22.5 cm range for Avanto setup without considerable change in the output voltage. This is larger than the typical MRI coil size, thus offering a considerable degree of freedom in placing the harvesting coil. The measurements show that it is possible to increase output voltage almost two times at the harvesting output with circularly polarized RF-coil. Still, the overall efficiency depends on the value of the load. Further details are given in Supplementary Materials.

Next, we study the RF field B_1 inside the body phantom for different locations of the harvesting coil to ensure that it does not impact the MRI functionality. The axial cross-section of B_1 field in (xy)-plane at the isocenter $z = 0$ for Espree MRI scanner with a body phantom is shown in Fig. 4(b). In such a case, no harvesting coil is present, and the magnetic field appears nearly homogeneous up to some noise which is caused mostly by the pulse sequence chosen for B_1 measurement within the applied technique [33]. Then, if the harvesting coil is introduced in the close vicinity of the phantom's surface at the distance of 1 cm, the field B_1 considerably changes (see Fig. 4(c)). In particular, the presence of coil leads to the emergence of inhomogeneity at the right side of the phantom. The field pattern becomes asymmetric due to several reasons, including the mirror asymmetry of the harvesting coil itself since the tuning capacitors and rectifiers are introduced in a non-symmetric fashion. However, if the distance between the harvesting coil and the phantom reaches 5 cm, then the field again appears unperturbed, as shown in Fig. 4(d), and closely resembles that in the absence of harvesting coil, Fig. 4(b). This said the proposed harvesting coil design should not affect the quality of MRI images if placed at sufficient separation from the patient.

The peak voltage during one RF excitation pulse reaches up to 100 V on the $R = 200$ Ohm load. Therefore, the peak power is approximately 50 W. However, the duration of excitation pulses usually in the range 100 μs - 5 ms, and time repetition (TR) pulse time is typically from 5 ms to several seconds [34]. Besides, the envelope shape of MR-signal is not a rectangle, as sinc-function is mostly used. As a result, the estimated av-

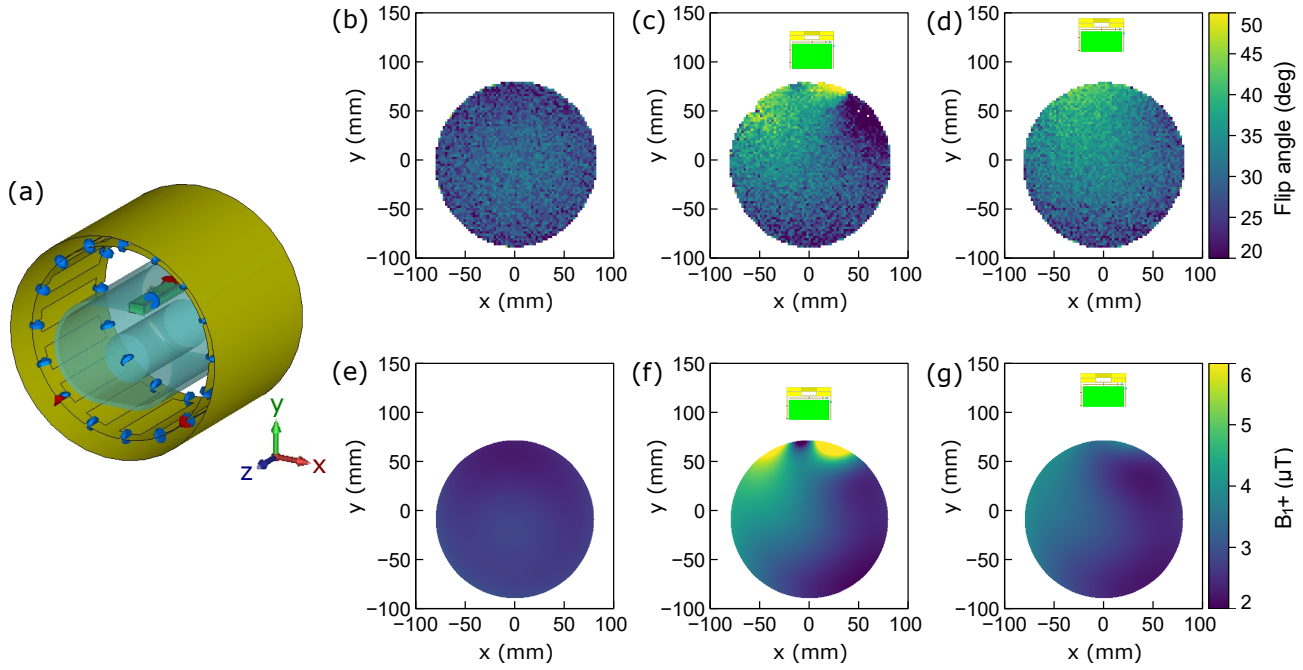


Figure 4. (a) The numerical model implemented in CST Microwave Studio. Blue cylinder and frame correspond to the water-filled body phantom. BC and scanner edge are shown with yellow, while blue disks denote capacitors placed in birdcage coil. The harvesting coil is placed atop the phantom. Red arrows show the location of ports used in numerical simulation. Maps of the RF magnetic fields B_1 in the (xy)-plane for $Z = 0$ obtained numerically (e-g) and experimentally (b-d) for the phantom without harvesting coil (b,e), with harvesting coil located at the height $h = 1$ cm above the phantom (c,f), and with harvesting coil located at the height $h = 5$ cm above the phantom (d,g).

erage power at each step of the phase encoding cycle is about 100...500 mW.

IV. NUMERICAL SIMULATIONS

To further detail our studies, we perform a set of numerical simulations with CST Microwave Studio 2020. First, we repeat the experimental protocols starting with harvesting output voltage depends on the distance z shown with solid green curve in Fig. 3(c). For such a simulation, we create a model that incorporates a birdcage body coil, homogeneous cylindrical phantom with additional frame resembling the ones used in real experiments, and a detailed model of the harvesting coil, including necessary lumped elements, Fig. 4(a). As seen from Fig. 3(c), numerical simulation results agree well with both Espree and Avanto measurements. However, numerically obtained voltages are greater than experimental ones in the vicinity of isocenter up to 10%, which is likely related to the simplified nature of the model does not taking into account realistic body coil design features (such as additional slots with serial capacitors) required for eliminating eddy currents.

Then, we calculate the root mean square (RMS) of the RF field B_1 in the absence of the harvesting coil, Fig. 4(e), and for the harvesting coil located at different distances from the phantom. Fig. 4(f,g) applying the same numerical model. As seen from the obtained distributions, the field with the harvesting coil placed at the distance 5 cm closely resembles that in the absence of coil, while for the coil located at 1 cm the field appears strongly perturbed. These results demonstrate good agreement with the experiment.

The safety of MRI is mostly defined by the SAR, which identifies the amount of RF radiation absorbed by the patient. To verify the patient safety in the presence of the harvesting coil, we perform numerical simulations of SAR. For this, we employ the detailed voxel 3D model of a human body, including internal organs and perform simulations in CST Microwave Studio with the same body and harvesting coil, Fig. 5(a). In Fig. 5(b), SAR is calculated in the absence of the harvesting coil. The resulting pattern appears asymmetric with a maximum in one hand of the patient. If the harvesting coil placed close to the patient at a distance 1 cm, that SAR decreases due to the presence of absorption in the coil, highlighting the absence of sufficient field value focusing in the region of patient, Fig. 5(c). Finally, if the harvesting coil is located at 5 cm above the patient as shown in Fig. 5(d), then SAR distribution becomes close to the one observed in the absence of coil, still featuring no pronounced increase. Thus, the proposed harvesting coil design appears safe for MRI applications.

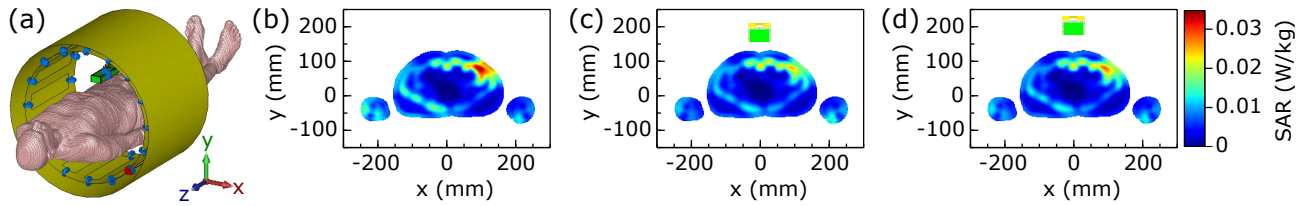


Figure 5. (a) Voxel model of a human used for numerical simulations of the specific absorption rate (SAR), (b-d) SAR images in the case without harvesting coil (b) and with a harvesting coil placed at the height of 1 cm (c) and 5 cm (e) above the voxel model.

V. DISCUSSION

We have developed a novel design of harvesting coil for MRI based on the use of two decoupled coils to convert circularly polarized RF field in contrast to linear polarization harvesters developed previously. Such a modification appears natural due to the circular polarization of the field B_1 created by the birdcage body coil. The measurements show that it is possible to increase output voltage almost two times with circularly polarized RF-coil. By performing numerical simulations and experiments with real MRI scanners, we demonstrate that the proposed coil is suitable for low power consumption devices, safe for the patient, and does not considerably affect the homogeneity of the RF magnetic field.

The proposed design can be used as a main or additional power supply for multichannel phased array coils, which are the gold standard in clinical MRI imaging. The amount of channels there can achieve high numbers up to 8 or even higher. Each channel requires power levels of at least [2] 100-300 mW. Therefore for the proper functioning of 8 channel array, about 3 W would be required, which is unattainable for the current harvesting setup. However, based on our design, it is possible to realize 1-2 channel wireless coil (for example, for dental MRI [35]), MRI coil wireless identification, wireless ECG sensors [36], etc. The directions for further development of the concept include direct testing of harvesting coil use in combination with local coils and sensors.

ACKNOWLEDGMENTS

This work was supported by the Russian Science Foundation (Project No.21-79-30038).

[1] Lena Nohava, Jean-Christophe Ginefri, Georges Willoquet, Elmar Laistler, and Roberta Frass-Kriegl, "Perspectives in wireless radio frequency coil development for magnetic resonance imaging," Frontiers in Physics **8** (2020), 10.3389/fphy.2020.00011.

[2] Kelly Byron, Fraser Robb, Pascal Stang, Shreyas Vasanawala, John Pauly, and Greig Scott, "An rf-gated wireless power transfer system for wireless mri receive arrays," Concepts in Magnetic Resonance Part B: Magnetic Resonance Engineering **47**, e21360 (2017).

[3] Mingzhao Song, Pavel Smirnov, Ekaterina Puhtina, Esmaeel Zanganeh, Stanislav Glybovski, Pavel Belov, and Polina Kapitanova, "Multi-mode metamaterial-inspired resonator for near-field wireless power transfer," Applied Physics Letters **117**, 083501 (2020).

[4] Kelly Byron, Chris Ellenor, Fraser Robb, Shreyas Vasanawala, John Pauly, and Greig Scott, "Mri compatible wireless power transfer system," in *Proceedings of the 22nd Annual Meeting of ISMRM*, Vol. 925 (2014).

[5] Kelly Byron, Simone A. Winkler, Fraser Robb, Shreyas Vasanawala, John Pauly, and Greig Scott, "An MRI compatible RF MEMs controlled wireless power transfer system," IEEE Transactions on Microwave Theory and Techniques **67**, 1717–1726 (2019).

[6] Aasrith Ganti, Jenshan Lin, Tracy Wynn, and Timothy Ortiz, "Achieving electromagnetic compatibility of wireless power transfer antennas inside MRI system," Wireless Power Transfer **6**, 138–153 (2019).

[7] Mingzhao Song, Ivan Iorsh, Polina Kapitanova, Elizaveta Nenasheva, and Pavel Belov, "Wireless power transfer based on magnetic quadrupole coupling in dielectric resonators," Applied Physics Letters **108**, 023902 (2016).

[8] Mingzhao Song, Pavel Belov, and Polina Kapitanova, "Wireless power transfer based on dielectric resonators with colossal permittivity," Applied Physics Letters **109**, 223902 (2016).

[9] Viacheslav Ivanov, Alena Shchelokova, Anna Andreychenko, and Alexey Slobozhanyuk, "Coupled very-high permittivity dielectric resonators for clinical mri," Applied Physics Letters **117**, 103701 (2020).

[10] Jens Höfflin, Elmar Fischer, Jürgen Hennig, and Jan G Korvink, "Energy harvesting towards autonomous mri detection," in *Proceedings of the International Society for Magnetic Resonance in Medicine*, Vol. 21 (2013) p. 728.

[11] Mehmet Bakir, Muharrem Karaaslan, Olcay Altintas, Mehmet Bagmanci, Volkan Akdogan, and Feyzullah Temurtas, "Tunable energy harvesting on uhf bands especially for gsm frequencies," International Journal of Microwave and Wireless Technologies **10**, 67 (2018).

[12] Triet Le, Karti Mayaram, and Terri Fiez, "Efficient far-field radio frequency energy harvesting for passively powered sensor networks," IEEE Journal of solid-state circuits **43**, 1287–1302 (2008).

[13] Taeho Oh, Omiya Hassan, Samira Shamsir, and Syed K Islam, "Low-power rf energy harvester circuit design for wearable medical applications," in *2019 United States National Committee of URSI National Radio Science Meeting (USNC-URSI NRSM)* (IEEE, 2019) pp. 1–2.

[14] KKA Devi, Md Din Norashidah, Chandan Kumar Chakrabarty, and S Sadasivam, "Design of an rf-dc conversion circuit for energy harvesting," in *2012 IEEE International Conference on Electronics Design, Systems and Applications (ICEDSA)* (IEEE, 2012) pp. 156–161.

[15] Yunus Uzun and Erol Kurt, "Design and simulation of a new dual-band rf energy harvester with high efficiency," in *2015 International Symposium on Consumer Electronics (ISCE)* (IEEE, 2015) pp. 1–2.

[16] Chong Huang, Xiaochen Gu, Lei Cai, Cong Li, Dun Yan, Bingbing Zhang, Qin Qin, Hongyi Wang, and Jiancheng Li, "An adaptive q factor tuning and input impedance matching method for ultra-low power front end of uhf rfid tag," in *2013 IEEE 10th International Conference on ASIC* (IEEE, 2013) pp. 1–4.

[17] Mohsen Shahmohammadi, Matt Chabalko, and Alanson P Sample, "High-q, over-coupled tuning for near-field rfid systems," in *2016 IEEE International Conference on RFID (RFID)* (IEEE, 2016) pp. 1–8.

[18] Ekkaphol Khansalee, Yan Zhao, and Kittipong Nuanyai, "High frequency rectifier for rf energy harvesting systems," in *2015 7th International Conference on Information Technology and Electrical Engineering (ICITEE)* (IEEE, 2015) pp. 304–308.

[19] Syeda Wajiha Munir, Osama Amjad, Engin Zeydan, and Ali Özer Ercan, "Optimization and analysis of wlan rf energy harvesting system architecture," in *2016 International Symposium on Wireless Communication Systems (ISWCS)* (IEEE, 2016) pp. 429–433.

[20] Marco Fantuzzi, Mohammad Rajabi, Gustavo Avolio, Alessandra Costanzo, and Dominique Schreurs, "Large signal rectifier characterization for simultaneous data and power transfer," in *2016 IEEE Wireless Power Transfer Conference (WPTC)* (IEEE, 2016) pp. 1–4.

[21] Long Li, Xuanming Zhang, Chaoyun Song, and Yi Huang, "Progress, challenges, and perspective on metasurfaces for ambient radio frequency energy harvesting," Applied Physics Letters **116**, 060501 (2020).

[22] Manuel Piñuela, Paul D Mitcheson, and Stepan Lucyszyn, "Ambient rf energy harvesting in urban and semi-urban environments," IEEE Transactions on microwave theory and techniques **61**, 2715–2726 (2013).

[23] Simon Hemour and Ke Wu, "Radio-frequency rectifier for electromagnetic energy harvesting: Development path and future outlook," Proceedings of the IEEE **102**, 1667–1691 (2014).

[24] Sangkil Kim, Rushi Vyas, Jo Bito, Kyriaki Niotaki, Ana Collado, Apostolos Georgiadis, and Manos M Tentzeris, "Ambient rf energy-harvesting technologies for self-sustainable standalone wireless sensor platforms," Proceedings of the IEEE **102**, 1649–1666 (2014).

[25] J. Thomas Vaughan, Carl J. Snyder, Lance J. DelaBarre, Patrick J. Bolan, Jinfeng Tian, Lizann Bolinger, Gregor Adriany, Peter Andersen, John Strupp, and Kamil Ugurbil, "Whole-body imaging at 7t: Preliminary results," Magnetic Resonance in Medicine **61**, 244–248 (2009), https://onlinelibrary.wiley.com/doi/pdf/10.1002/mrm.21751.

[26] Bernhard Gruber, Martijn Froeling, Tim Leiner, and Dennis W.J. Klomp, "Rf coils: A practical guide for nonphysicists," Journal of Magnetic Resonance Imaging **48**, 590–604 (2018), https://onlinelibrary.wiley.com/doi/pdf/10.1002/jmri.26187.

[27] E Mark Haacke, Robert W Brown, Michael R Thompson, Ramesh Venkatesan, *et al.*, *Magnetic resonance imaging: physical principles and sequence design*, Vol. 82 (Wiley-liss New York:, 1999).

[28] Mathias Blasche, "Gradient performance and gradient amplifier power," Magnetom Flash **69**, 244–248 (2017).

[29] CPC Amps, Inc., *Introduction to NMR/MRI RF Amplifiers* (http://www.cpcamps.com/introduction-to-nmr-mri-amplifiers.html, 2012).

[30] Siemens, *Operator Manual Magnetom Prisma*, Vol. 1 (https://www.siemens-healthineers.com/, 2018).

[31] MJ Riffe, JA Heilman, and MA Griswold, "Power scavenging circuit for wireless dc power," in *Proc. Intl. Soc. Mag. Reson. Med*, Vol. 15 (2007) p. 3273.

[32] Michael Twieg, Michael A de Rooij, and Mark A Griswold, "Active detuning of mri receive coils with gan fets," IEEE Transactions on Microwave Theory and Techniques **63**, 4169–4177 (2015).

[33] EK Insko and L Bolinger, "Mapping of the radiofrequency field," Journal of Magnetic Resonance, Series A **103**, 82–85 (1993).

[34] Matt A Bernstein, Kevin F King, and Xiaohong Joe Zhou, *Handbook of MRI pulse sequences* (Elsevier, 2004).

[35] Ute Ludwig, Anne-Katrin Eisenbeiss, Christian Scheifele, Katja Nelson, Michael Bock, Jürgen Hennig, Dominik Von Elverfeldt, Olga Herdt, Tabea Flügge, and Jan-Bernd Hövener, "Dental mri using wireless intraoral coils," Scientific reports **6**, 1–11 (2016).

[36] Mirza Mansoor Baig, Hamid Gholamhosseini, and Martin J Connolly, "A comprehensive survey of wearable and wireless ecg monitoring systems for older adults," Medical & biological engineering & computing **51**, 485–495 (2013) .